PACS 87.50.W-

Correlation optical microscopy of anisotropic biological layers

A.G. Ushenko, A.V. Dubolazov, Yu.A. Ushenko, M.Yu. Sakhnovskiy, O.V. Olar, A.V. Motrich, P.O. Angelsky
Chernivtsi National University,
2, Kotsyubinsky str., 58012 Chernivtsi, Ukraine;
E-mail: a.dubolazov@chnu.edu.ua

Abstract. The theoretical background of an azimuthally stable method for Jones-matrix mapping histological sections of biopsy taken from myocardium tissue on the basis of spatial frequency selection of mechanisms responsible for linear and circular birefringence is presented. The diagnostic application of a new correlation parameter – complex degree of mutual anisotropy – has been analytically substantiated. The method for measuring coordinate distributions of complex degree of mutual anisotropy with further spatial filtration of their high- and low-frequency components has been developed. The interrelations of these distributions with parameters of linear and circular birefringence in myocardium tissue histological sections have been found. The comparative results of measuring the coordinate distributions inherent to complex degree of mutual anisotropy related with fibrillar networks of myosin fibrils typical for myocardium tissue in different necrotic states, when death is caused by coronary heart disease and acute coronary insufficiency, have been presented. The values and ranges of changes in the statistical (moments of the 1st to 4th order) parameters describing the complex degree of mutual anisotropy coordinate distributions have been studied. The objective criteria for differentiation of causes leading to death have been determined.

Keywords: polarization, Fourier optics and signal processing, imaging systems, medical and biological imaging.

Manuscript received 11.11.16; revised version received 18.01.17; accepted for publication 01.03.17; published online 05.04.17.

1. Mueller-matrix formalism as the basis of correlation polarimetry

1.1. Introduction

Methods of optical diagnostics of biological tissues (BT) include three main directions:

- Spectral methods [1-3] based on investigation of absorption spectra inherent to biological objects and media.
- Polarization methods [4-7]. The main disadvantage of polarization methods consists in the azimuthal dependence of the obtained data on the rotation angle of the sample relatively to the probing beam [4, 8-11]. Therefore, the results of polarization mapping are hard to be reproduced.
- The correlation "two-points" methods are devoid of this disadvantage [12-14]. In [15] for characterizing the consistency between the polarization states the object field in the points (d_1, d_2) with the intensities $I(d_1, t)$, $I(d_2, t)$ a new azimuthally stable parameter – complex degree of mutual polarization (CDMP) $W(d_1, d_2, t)$ – was introduced

$$W(d_1, d_2) = \frac{\left(E_x(d_1)E^*{}_x(d_2) + E_y(d_1)E^*{}_y(d_2)\right)^2}{I(d_1)I(d_2)}. \quad (1)$$

For practical use in the field of investigation of optically anisotropic tissues, one should use the following form of equation (1) [16-19]

$$\mathrm{Re}\{W\} \equiv \tilde{W}(d_1, d_2) = \\ = \frac{\left\{E_x(d_1)E_x(d_2) - E_y(d_1)E_y(d_2)\cos[\theta(d_1) - \theta(d_2)]\right\}^2}{I(d_1)I(d_2)}, \tag{2}$$

where $\theta(d_1)$ and $\theta(d_2)$ are the phase shifts between the orthogonal components E_x, E_y of laser beam amplitude.

In [16-19], Eq. (2) takes into consideration linear birefringence in fibrillar networks of biological tissues. Along with this topical task, taken into account is circular birefringence of protein molecules that form fibrillar networks. The technique proposed in [20] enables to separate manifestations of these anisotropy mechanisms by means of usage the technique of direct and inverse Fourier transforms applied to microscopic images of these objects.

This research presents the possibilities to diagnose myocardium necrotic changes. Up to date, postmortem diagnostics of acute coronary syndrome is a leading approach in morphological [21, 22] and forensic [23, 24] medical investigations. The balanced accuracy [25-39] of acute coronary insufficiency detection by conventional histochemical methods does not exceed 65…70% and takes relatively long time. Therefore, topical is the development of new, more accurate and express methods for applying novel optical-physical approaches to formation and processing of microscopic images of myocardium histological sections.

This work is aimed to develop and substantiate the method of "two-point" Jones-matrix mapping and spatial-frequency filtering for manifestations of optical anisotropy caused by the necrotic changes in histological sections of myocardium tissue of those people who died of ischemic heart disease (IHD) and acute coronary insufficiency (ACI).

1.2. Theory

Biological tissues simultaneously join the following two types of optical anisotropy [10]:

- phase anisotropy (linear and circular birefringence),
- amplitude anisotropy (linear and circular dichroism).

Optical manifestations of the respective mechanisms are related with the morphological structure of biological tissues. In this way, circular birefringence and dichroism are related with the spiral-like structure of protein molecules. Similarly, linear birefringence and dichroism are caused by these molecules spatially ordered in fibrillar networks.

Mechanisms of phase and amplitude anisotropies can be separated by choosing the appropriate spectral region. Protein absorption is minimal in the long-wave spectral region. Due to this, in our spectral region of He-Ne laser emission (λ = 0.6328 μm) optical anisotropy of myocardium can be represented by combination of circularly birefringent myosin molecules, which form linearly birefringent fibers and bundles of fibrillar network.

Let us consider in details the analytical description of the processes of laser radiation transformation in myocardium tissue as being based on the following assumptions [4, 6-11]:

- myocardium tissue consists of two optically anisotropic components with different scales of spatial organization;
- "small-scale" (l ~ 5…15 μm) complexes of optically anisotropic molecules of myosin with prevailing circular birefringence;
- "large-scale" fibrillar optically anisotropic network of myosin (range of transversal sizes l ~ 50…200 μm) with prevailing linear birefringence (due to ordering of packing that determines the directions of optical axes of partial biological crystals);
- polarization properties of the points of this optically anisotropic medium are characterized by the generalized matrix of optical anisotropy $\{F\}$

$$\{F\} = \{L\}\{C\}, \tag{3}$$

where $\{L\}$ is the Jones matrix of linear birefringence; $\{C\}$ – Jones matrix of circular birefringence or optical activity [19]

$$\begin{cases} f_{11} = \left[\sin^2\rho + \cos^2\rho\exp(-i\omega)\right]\cos\psi + \left[\sin\rho\cos\rho(1-\exp(-i\omega))\right]\sin\psi, \\ f_{12} = -\left[\sin^2\rho + \cos^2\rho\exp(-i\omega)\right]\sin\psi + \left[\sin\rho\cos\rho(1-\exp(-i\omega))\right]\cos\psi, \\ f_{21} = \left[\sin\rho\cos\rho(1-\exp(-i\omega))\right]\cos\psi + \left[\cos^2\rho + \sin^2\rho\exp(-i\omega)\right]\sin\psi, \\ f_{22} = -\left[\sin\rho\cos\rho(1-\exp(-i\omega))\right]\sin\psi + \left[\cos^2\rho + \sin^2\rho\exp(-i\omega)\right]\cos\psi. \end{cases} \tag{4}$$

Here, ρ is the direction of optical axis, $\omega = \left(2\pi/\lambda\right)\Delta np$ – value of phase shift between the orthogonal components of the amplitude of laser wave with the wavelength λ, which passed the geometrical path p through the biological crystal with linear birefringence Δn; ω – rotation angle of the polarization plane of the laser wave caused by circular birefringence.

Taking into account Exps (4) for azimuthally stable situation of biological tissue probing by circularly polarized beam, we gain the interrelation between the optical anisotropy of the tissue and the polarization structure of its image:

$$\begin{pmatrix} E_x(d) \\ E_y(r) \end{pmatrix} = \frac{1}{\sqrt{2}} \begin{Vmatrix} f_{11}(d) & f_{12}(d) \\ f_{21}(d) & f_{22}(d) \end{Vmatrix} \begin{pmatrix} 1 \\ i \end{pmatrix} = \\ = \frac{1}{\sqrt{2}} \begin{pmatrix} f_{11}(d) + if_{12}(d) \\ f_{21}(d) + if_{22}(d) \end{pmatrix}. \quad (5)$$

Relations (5) can be rewritten as a "single-point" interconnection of the amplitude and optically anisotropic parameters $\begin{cases} E_x(d) = g(\rho, \omega, \psi), \\ U_y(d) = j(\rho, \omega, \psi). \end{cases}$

Within the "two-point" approach [15-18], similarly to the CDMP parameter $W(d_1, d_2)$ (1), the Jones-matrix correlation parameter $H(d_1, d_2)$ – the complex degree of mutual anisotropy (CDMA) – can be introduced. It directly characterizes the degree of consistency between linear and circular birefringence of the points in the biological tissue $W\begin{pmatrix} E_x(d_1, d_2) \\ E_y(d_1, d_2) \end{pmatrix} \to H\begin{pmatrix} g(f_{ik}(d_1, d_2)) \\ j(f_{ik}(d_1, d_2)) \end{pmatrix}$. Therefore, to define the analytical expression for CDMA, we need to use the relation (1) and take into account the equations (3) to (5)

$$H(d_1, d_2) = \\ = \frac{\{f_{11}(d_1)f_{11}(d_2) + f_{12}(d_1)f_{12}(d_2) + f_{21}(d_1)f_{21}(d_2) + f_{22}(d_1)f_{22}(d_2)\}^2}{I(d_1)I(d_2)}. \quad (6)$$

Thus, we have obtained the relation for a new correlation parameter $H(d_1, d_2)$ that describes the generalized anisotropy of different layers in biological tissues. Let us determine the spatial-frequency filtering for separation of coordinate distributions of CDMA formed by various components of the diagnosed layer of myocardium tissue with linear and circular birefringence. From the viewpoint of medicine, the task of "optical selection" of polarization manifestations of the linear (ρ, ω) and circular (ψ) birefringence in the network of myosin fibrils of myocardium tissue is topical for differentiation of death causes. The matter is that, in the case of death caused by ACI, there are necrotic changes in myosin structures on a small-scale range. Optically, this process manifests itself in degradation of circular birefringence ($\psi \downarrow$) in the corresponding fibrillar network. In the case of death caused by IHD, it is accompanied by orientation changes of large-scale fibrillar network with the degradation of linear birefringence ($\omega \downarrow$). Conventional histological diagnostics and differentiation of these necrotic changes is rather labor-intensive, it requires more time and often appears to be ambiguous. For that, let us return to the analysis of interrelations ((1)-(6)) between the polarization structure of the image of biological layer and parameters describing its anisotropy. According to the suggested model of this anisotropy, linear birefringence is mainly typical for large-scale fibrillar networks of myosin fibrils. For small-scale structures of optically active molecules, circular birefringence is typical. Thus, spatially high-frequency ($E(\rho, \omega)$) and low-frequency ($E(\psi)$) components are formed in the image of this object. With the purpose to select these conditions, we have applied the method of spatial-frequency filtration of the polarization inhomogeneous laser images in the Fourier plane [20]. The main idea of this approach is that spatial-frequency structure of the Fourier form for the laser image of myocardium tissue is different for its large-scale and small-scale protein structures. Therefore, using spatial-frequency filtration it is mainly possible to isolate either low-frequency (with linear birefringence) or high-frequency (with circular birefringence) components, which by means of Fourier transform can be transformed into respectively "separated" laser images. If one locates the vignetting (transparent $L(\Delta\chi, \Delta\gamma)$ opaque $L^{-1}(\Delta\chi, \Delta\gamma)$) diaphragm in the central part of Fourier plane, then by means of reverse Fourier transform the low- and high-frequency components can be restored

$$\begin{cases} \hat{E}(\rho, \omega, \chi, \gamma) = L(\Delta\chi, \Delta\gamma)E(\chi, \gamma); \\ \hat{E}(\psi, \chi, \gamma) = L^{-1}(\Delta\chi, \Delta\gamma)E(\chi, \gamma). \end{cases}$$

Here, $\chi = \frac{x}{\lambda f}$ and $\gamma = \frac{y}{\lambda f}$ – spatial frequencies. Therefore, it is possible to determine the coordinate distributions of the Jones matrix elements of linear $q_{ik}(\rho, \omega) = F(\hat{U})$ and circular $a_{ik}(\psi) = F(\dot{U})$ birefringence according to the classical technique [19]. As a result, we obtain analytical expressions of the CDMA parameter for various types of optically anisotropic layers prepared from myocardium tissue $H(\rho, \omega, d_1, d_2)$ and $H(\psi, d_1, d_2)$.

Experimental confirmation of the efficiency of spatial-frequency separation of optical manifestations of mechanisms responsible for phase anisotropy observed in different-scale structures of myocardium is represented by symmetry of Jones matrix. Thus, for the linear birefringence all the matrix elements should be

$f_{ik} \neq 0$ (object field is formed by elliptically polarized parts). For circular birefringence, one can see the following relations: $f_{12;21} \to 0$, $f_{11} \approx f_{22}$ (object field is formed by linearly polarized parts).

1.3. Optical realization of spatial-frequency filtration for coordinate distributions of CDMA

Experimental investigations of CDMA coordinate distributions were performed using the classical polarimetry setup [5]. Fig. 1 presents a modified setup of such laser Stokes-polarimeter with spatial-frequency filtration.

Illumination of the investigated sample *6* was performed by parallel ($\varnothing = 10^4$ μm) He-Ne ($\lambda = 0.6328$ μm; power $W = 5$ mW) laser beam *1*, *2*. The polarization light source consists of quarter-wave plates *3*, *5* (Achromatic True Zero-Order Waveplate) and polarizer *4*; this enables to form a laser beam with random azimuth $0° \le \alpha_0 \le 180°$ or ellipticity $0° \le \beta_0 \le 90°$ of polarization. Histological sections of myocardium *6* were located in the focal plane of polarization micro-objective *7* (Nikon CFI Achromat P, focal distance – 30 mm, *NA* – 0.1, magnification – 4×). In the back focal plane a spatial-frequency (a low-frequency $L(\Delta\chi, \Delta\gamma)$ or high-frequency $L^{-1}(\Delta\chi, \Delta\gamma)$ one) filter *8* was placed. Polarization micro-objective *9* was located at the focal distance from the frequency plane of the objective *7* and, therefore, performed an inverse Fourier-transform of spatial-temporally filtered field of laser radiation. The coordinate distribution of this field intensity was registered in the plane of light-sensitive CCD-camera *12* (The Imaging Source DMK 41AU02.AS, monochrome 1/2" CCD, Sony ICX205AL (progressive scan); resolution – 1280×960; size of light-sensitive plate – 7600×6200 μm; sensitivity – 0.05 lx; dynamic range – 8 bit; SNR – 9 bit, deviation of photosensitive characteristics from the linear one does not exceed 12%) that was also located at the focal distance from the micro-objective *9* and provided the measurement range of the structural elements of the restored image for myocardium tissue histological sections within the range of geometrical sizes 2…2000 μm.

2. Polarization-correlation maps of biological layers

2.1. Materials and methods

The experimental measurement of CDMA components – complex elements d_{ik} of Jones matrix – is based on the approach suggested in [18].

2.1.1. Determination of statistically reliable representative selection of patients with the known (referent) diagnosis

As objects for investigations, we used optically thin (attenuation coefficient $\tau \approx 0.091…0.097$) histological sections of biopsy taken from myocardium tissue and prepared according to standard technique by using the freezing microtome. In this case, inside the volume of these layers single scattering regime is realized. In other words, there is no depolarization (multiple scattering) but transformation of polarization, which is accompanied by formation of polarization-inhomogeneous images of myocardium samples.

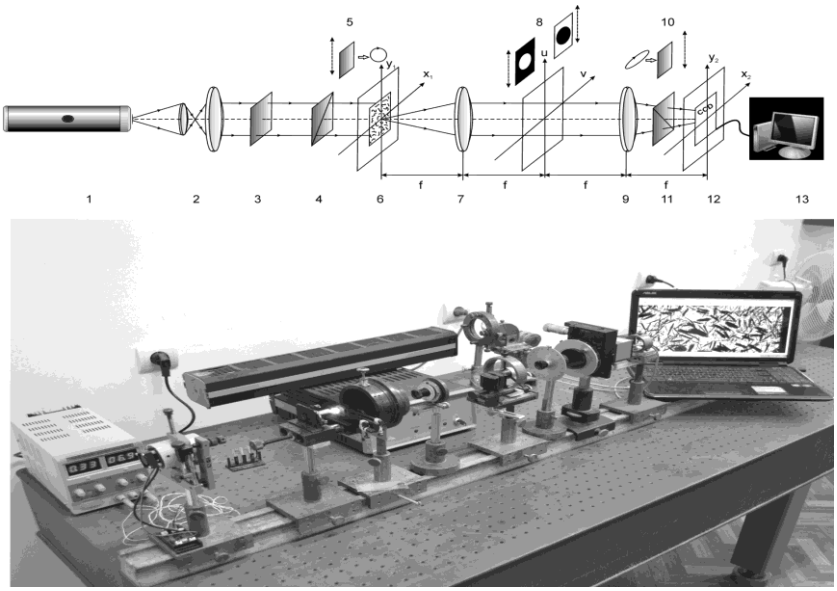

Fig. 1. Optical scheme of Stokes-polarimeter providing spatial-frequency filtration: *1* – He-Ne laser; *2* – collimator; *3* – stationary quarter-wave plate; *5*, *10* – mechanically movable quarter-wave plates; *4*, *11* – polarizer and analyzer, respectively; *6* – object of investigation; *7*, *9* – polarization micro-objectives; *8* – low-frequency and high-frequency filters, *12* – CCD camera; *13* – personal computer.

From the medical viewpoint, there were formed two groups of patients with the following diagnoses:

- group 1 – death caused by IHD;
- group 2 – death caused by ACI.

In our case, the group 1 was chosen as the reference one and group 2 – samples under investigation.

Differentiation of IHD (group 1) and ACI (group 2) was provided using the gold standard method – biopsy of surgically removed myocardium. By means of the software product Statmate, for 95% confidence interval ($p < 0.05$) a reliable quantity of people was determined as $n = 51$. The value of representative sampling was verified by the cross-check method. It was determined that the value of root-mean-square deviation of the average value of statistical moments $M_{i=1;2;3;4}$ does not exceed 0.025; it corresponds to the value of statistically reliable confidence interval $p < 0.05$.

2.1.2. Preparation of samples

Optically thin histological sections of myocardium tissue biopsy were prepared according to standard technique by using the freezing microtome.

2.1.3. Algorithms of the analysis of CDMA coordinate distributions

The measured distributions $q \equiv \{H_{\rho,\omega}, H_{\psi}\}$ were objectively assessed within the statistical approach – the set of statistical moments of the 1st to 4th orders

$$M_1 = \frac{1}{S}\sum_{j=1}^{S} q_j,$$

$$M_2 = \sqrt{\frac{1}{s}\sum_{j=1}^{S}(q - M_1)_j^2}, \; M_3 = \frac{1}{M_2{}^3}\frac{1}{S}\sum_{j=1}^{S}(q - M_1)_j^3,$$

$$M_4 = \frac{1}{M_2{}^4}\frac{1}{S}\sum_{j=1}^{S}(q - M_1)_j^4. \qquad (7)$$

Here, S is the number of pixels of CCD-camera. These parameters characterize the mean (M_1), dispersion (M_2), skewness (M_3) and kurtosis or "peak sharpness" (M_4) of histograms $N(q)$.

2.1.4. Jones-matrix mapping with spatial-frequency selection of CDMA coordinate distributions of myocardium histological sections

Being based on experimental measurements of Jones-matrix elements, we used an approach proposed in the classical monograph by Gerrard and Burch. There, the Jones matrix consists of two components – real and imaginary. The values of real components of Jones matrix elements can be measured as follows:

- sample was illuminated by linearly polarized beam with the azimuth 0°;
- transmission plane of analyzer was rotated by the angles of 0°, 90°, and the corresponding intensities of transmitted radiation were measured;
- sample was illuminated by linearly polarized beam with the azimuth 90°;
- transmission plane of analyzer was rotated by the angles of 0°, 90°, and the corresponding intensities of transmitted radiation were measured;
- real components of Jones matrix elements were calculated.

The values of imaginary components of Jones matrix elements can be measured as follows:

- sample should be illuminated by right circularly polarized beam (angle between the transmission plane of polarizer and fast axis of the quarter-wave plate should be 45°);
- transmission plane of analyzer should be rotated by the angles of 0°, 90°, and the corresponding intensities of transmitted radiation must be measured;
- sample should be illuminated by linearly polarized beam with the azimuth 45°;
- transmission plane of analyzer should be rotated by the angles of 0°, 90°, and the corresponding intensities of transmitted radiation must be measured;
- imaginary components of Jones matrix elements are to be calculated.

For the purpose of choosing the diaphragm size, the dependences of values for all the statistical moments on the size of spatial-frequency diaphragm were investigated. It was determined that, beginning from the specific size of spatial-frequency filter (ΔR = 125 pix), the change of values of the set of statistical moments reached its saturation. As the criterion of optimal size, we chose the condition of simultaneous extreme values of all the statistical moments. For low-frequency filter (transparent), the diaphragm size was ΔR = 30 pix – transmission of spatial frequencies up to $\nu = 10\ \text{mm}^{-1}$. The optimal size of high-frequency filter (opaque) was ΔR^{-1} = 60 pix – transmission of spatial frequencies from $\nu = 20\ \text{mm}^{-1}$.

The efficiency of spatial-frequency filtering manifestations of linear and circular birefringence was estimated in accordance with symmetry of Jones matrixes and prevailing polarization type of high- and low-frequency components for images of myocardium samples.

It was determined that in the case of low-frequency filtering all the elements of Jones matrix $f_{ik} \neq 0$. In addition, 94% of the pixels of digital camera recorded elliptically polarized areas of the myocardium image. In the case of high-frequency filtering, the following results were obtained – $f_{12;21} \to 0$; $f_{11} \approx f_{22}$ (91% of linearly polarized areas).

The values of CDMA were calculated as follows:

- under different diaphragming conditions, the two-dimensional arrays of values inherent to Jones matrix elements were measured within each pixel;
- for each line in two-dimensional array of Jones matrix elements, pairs of neighbor pixels were chosen;

- for each pair of these pixels one value of CDMA was calculated;
- at the next stage by means of scanning with the step of one pixel, a set of CDMA values was determined within the chosen line of CCD camera;
- above mentioned scanning was performed within all the lines of light sensitive area in CCD camera and the two-dimensional array of CDMA values was calculated.

2.2. Polarization-correlation maps

Figs. 2 and 3 present the results of Jones-matrix mapping for low-frequency (linear birefringence of fibrillar networks – Fig. 2) and high-frequency (circular birefringence of myosin molecules – Fig. 3) CDMA distributions of myocardium tissue histological sections. Figures contain the coordinate distributions (fragments (1), (3)) and histograms $N(q)$ (fragments (2), (4)) of sample randomly taken from the group 1 (fragments (1), (2)) and from group 2 (fragments (3), (4)).

CDMA $H_{\rho,\omega}$. The comparative analysis of the spatial-frequency filtered coordinate distributions $H_{\rho,\omega}(m\times n)$ for the large-scale network of myocardium layer revealed certain difference between them. The histograms of the CDMA distribution for a histological section of myocardium from the group 2 (ACI) are characterized by an asymmetric structure (Fig. 2, fragment (4)). The similar distribution found for the tissue sample from group 1 (IHD) (Fig. 2, fragment (2)) is more symmetrical. The revealed peculiarity is related to the structure of myosin fibrils. For histological sections of the group 2, the directions of the myosin fibrils are more ordered in the direction of optical axes. For the samples from the group 1, the similar network of myocardium layer is more disordered in directions. Optically, this geometrical structure ($\rho^* \leftrightarrow N_{\max}$) is revealed in formation of the priority, most probable values of CDMA $H_{\rho,\omega}(m\times n)$ (relations (1), (3)-(6)), the set of which forms the main extreme. Statistically, this process is detected by the following changes in $M_{i=1;2;3;4}(H_{\rho,\omega})$ (relations (7)). For IHD – the decrease of the skewness $M_3\downarrow$ and the kurtosis $M_4\downarrow$ of histograms $N(H_{\rho,\omega})$. Other statistical moments (mean $M_1\uparrow$, dispersion $M_2\uparrow$) increase. Thus, "CDMA $H_{\rho,\omega}$-biopsy" appeared to be sensitive to the changes of linear birefringence caused by necrotic transformation of fibrillar networks of myocardium. That is why this

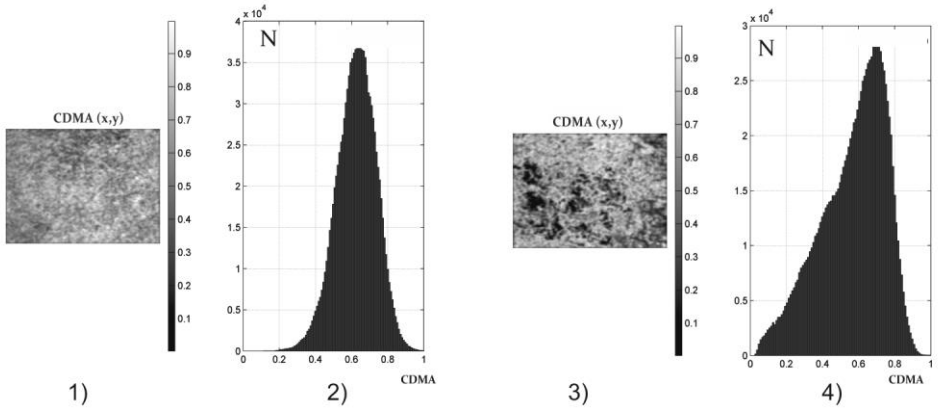

Fig. 2. Coordinate structure ((1), (3)) and histograms ((2), (4)) of CDMA distributions of linear birefringence in histological sections of biopsy taken from myocardium tissue of the groups 1 ((1), (2)) and 2 ((3), (4)).

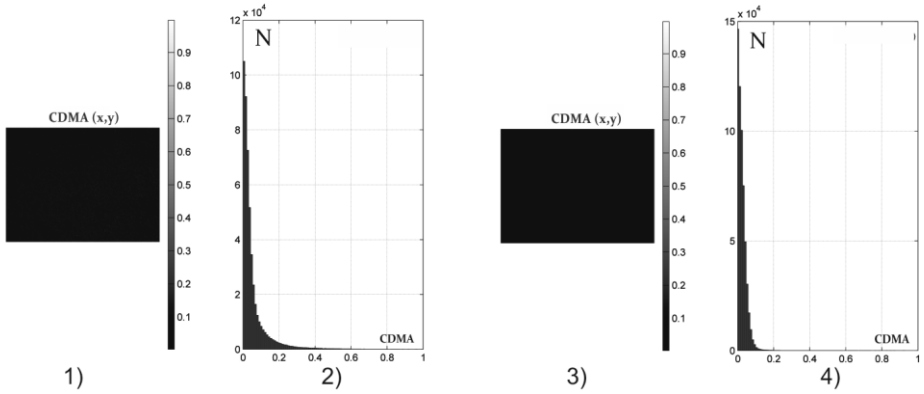

Fig. 3. Coordinate structure ((1), (3)) and histograms ((2), (4)) of CDMA distributions of circular birefringence in histological sections of biopsy taken from myocardium tissue of the groups 1 ((1), (2)) and 2 ((3), (4)).

information is important for differentiation of causes for death caused by IHD and ACI.

CDMA H_ψ. The physical mechanism of circular birefringence formation is first of all related to the concentration of optically active protein molecules of myosin, which form the myocardium fibrillar networks. Necrotic changes caused by ACI lead to decrease of concentration of protein molecules. Thus, the correlation parameter W_θ of these layers is characterized by the less magnitude of values in comparison with the CDMA distribution obtained for myocardium from the group 1. Quantitatively, this difference is characterized by histograms $N(H_\psi)$ (Fig. 3, fragment (2)). It is obvious from the obtained data (Fig. 3, fragment (4)) that for necrotic changes caused by ACI the decrease in magnitude values of the average $M_1(H_\psi)\downarrow$ and dispersion $M_2(H_\psi)\downarrow$ are typical. The skewness $M_3(H_\psi)\uparrow$ and kurtosis $M_4(H_\psi)\uparrow$ of distributions $N(H_\psi)$ increases. This fact indicates to sensitivity "CDMA H_ψ-biopsy" to "concentration" changes of circular birefringence in myocardium. That is why this information is the most important in the ACI diagnostics of myocardium.

2.3. Statistical intergroup analysis

Differentiation between the groups 1 and 2 was reached by using the following methodology [25-27]:

- within each set of values of statistical moments $M_{i=1;2;3;4}$, we determined the average value $\overline{M}_{i=1;2;3;4}$ and standard deviation $\sigma_{i=1;2;3;4}$;
- differences between the statistical sets $M_{i=1;2;3;4}$ were significant in the case when the average value $\overline{M}_{i=1;2;3;4}$ within the group 1 didn't "overlap" with the standard deviation $\sigma_{i=1;2;3;4}$ within the group 2, and *vice versa*;
- within both groups of myocardium samples, for the distributions of values of each statistical moments $M_{i=1;2;3;4}$ we chose cutoff of 3σ (99.72% of all the possible values of changes in M_i). Sequentially, we determined the number of "false negative" (*b*) and "false positive" (*d*) conclusions;
- for every statistical moments traditional for probative medicine operational characteristics: sensitivity $\left(Se = \frac{a}{a+b}100\%\right)$, specificity $\left(Sp = \frac{c}{c+d}100\%\right)$ and balanced accuracy $\left(Ac = \frac{Se+Sp}{2}\right)$, where *a* and *b* are the number of correct and wrong diagnoses within group 2; *c* and *d* – the same within the group 1 were determined.

The comparative analysis of the data obtained (Table 1) showed that the differences between the values of average $\overline{M}_{i=1;2;3;4}$ moments of all orders are statistically reliable. However, there is an intergroup overlap for all histograms $N(M_i)$. Moreover, the range of such an overlap is inversely proportional to the value of the difference between the averages $\overline{M}_{i=1;2;3;4}$. The moments $M_{i=3;4}(H_{\rho,\omega})$ appeared to be sensitive in differentiation of linear birefringence maps $H_{\rho,\omega}(m\times n)$ of myocardium histological sections (highlighted in grey in Table 1). For circular birefringence distributions $H_\psi(m\times n)$ of myocardium layers, the most preferable are statistical moments of higher orders $M_{i=3;4}(H_\psi)$.

Table 2 presents the parameters of information value of azimuthally stable method of Jones-matrix mapping for optical anisotropy of histological sections taken from myocardium with different necrotic changes.

The obtained results enable to state a rather high level of accuracy of azimuthally stable Jones-matrix mapping. According to the criteria of probative medicine

Table 1. Parameters of statistical structure of CDMA coordinate distributions.

Parameters	$H_{\rho,\omega}$		H_ψ	
	IHD	ACI	IHD	ACI
M_1	0.78±0.054	0.71±0.051	0.07±0.005	0.05±0.004
M_2	0.22±0.014	0.25±0.015	0.13±0.007	0.07±0.006
M_3	0.37±0.023	0.24±0.016	0.71±0.057	1.21±0.084
M_4	0.63±0.035	0.76±0.15	1.28±0.091	1.98±0.14

Table 2. Operational characteristics of the method of Jones-matrix mapping for optical anisotropy of histological sections taken from myocardium.

Parameters	M_i	$H_{\rho,\omega}$,%	H_ψ,%
$Ac(M_i)$	M_1	60	71
	M_2	55	67
	M_3	95	87
	M_4	90	93

[25], the parameters $Ac(\psi) \sim 90\%$ correspond to good quality, while $Ac(\rho, \omega) > 90\%$ – to high quality.

Conclusion

The comparative investigations of the effectiveness of the developed technique based on spatial-frequency Fourier polarimetry of CDMA in the diagnostics of necrotic changes in myocardium tissue are carried out.

The criteria of differentiation between the causes of death caused by IHD and ACI on the basis of the statistical (statistical moments of the 1st to 4th orders) analyses of the spatial-frequency filtered distributions of CDMA for protein networks with linear and circular birefringence have been determined.

Acknowledgement

This work was supported by the grant №0116U001446, №0116U001449, №0115U003241, №0115U003227, №0115U003235 from the Ukraine Foundation for Basic Research.

References

1. Tuchin V.V. *Tissue Optics: Light Scattering Methods and Instruments for Medical Diagnosis*, Second edition. PM 166, SPIE Press, Bellingham, WA, 2007.
2. Wang X., Yao G., Wang L.-H. Monte Carlo model and single-scattering approximation of polarized light propagation in turbid media containing glucose. *Appl. Opt*. 2002. **41**. P. 792–801.
3. Wang X., Wang L.-H. Propagation of polarized light in birefringent turbid media: A Monte Carlo study. *J. Biomed. Opt*. 2002. **7**. p. 279–290.
4. Angelsky O.V., Bekshaev A.Ya., Maksimyak P.P., Maksimyak A.P., Hanson S.G., Zenkova C.Yu. Self-action of continuous laser radiation and Pearcey diffraction in a water suspension with light-absorbing particles. *Opt. Exp*. 2014. **22**, No. 3. P. 2267–2277.
5. Cheong W.-F., Prahl S.A., Welch A.J. A review of the optical properties of biological tissues. *IEEE J. Quantum Electron*. 1990. **26**. P. 2166–2185.
6. Angelsky O.V., Bekshaev A.Ya., Maksimyak P.P., Maksimyak A.P., Hanson S.G., Zenkova C.Yu. Self-diffraction of continuous laser radiation in a disperse medium with absorbing particles. *Opt. Exp*. 2013. **21**, No. 7. P. 8922–8938.
7. Angel'skii O.V., Ushenko A.G., Arkhelyuk A.D., Ermolenko S.B., Burkovets D.N. Scattering of laser radiation by multifractal biological structures. *Optics and Spectroscopy*. 2000. **88**, No. 3. P. 444–447.
8. Angelsky O.V., Bekshaev A.Ya., Maksimyak P.P., Maksimyak A.P., Hanson S.G. Measurement of small light absorption in microparticles by means of optically induced rotation. *Opt. Exp*. 2015. **23**, No. 6. P. 7152–7163.
9. Ushenko Yu.A., Boychuk T.M., Bachynsky V.T., Mincer O.P. Diagnostics of structure and physiological state of birefringent biological tissues: Statistical, correlation and topological approaches, in: *Handbook of Coherent-Domain Optical Methods*. Springer Science+Business Media, New York, 2013. P. 107–148.
10. Ushenko Yu.A. Investigation of formation and interrelations of polarization singular structure and Mueller-matrix images of biological tissues and diagnostics of their cancer changes. *J. Biomed. Opt.* 2011. **16**. P. 066006.
11. Angelsky O.V., Besaha R.N., Mokhun A.I., Mokhun I.I., Sopin M.O., Soskin M.S., Vasnetsov M.V. Singularities in vectoral fields. *Proc. SPIE*. 1999. **3904**. P. 40.
12. Wolf E. Unified theory of coherence and polarization of random electromagnetic beams. *Phys. Lett. A*. 2003. **312**. P. 263–267.
13. Tervo J., Setala T., Friberg A. Degree of coherence for electromagnetic fields. *Opt. Exp.* 2003. **11**. P. 1137–1143.
14. Angelsky O.V., Tomka Yu.Ya., Ushenko A.G., Ushenko Y.G., Yermolenko S.B. 2-D tomography of biotissue images in pre-clinic diagnostics of their pre-cancer states. *Proc. SPIE*. 2005. **5972**. P. 158–162.
15. Ushenko A.G., Angelsky P.O., Sidor M.I., Marchuk Yu.F., Andreychuk D.R., and Pashkovskaya N.V. Spatial-frequency selection of complex degree of coherence of laser images of blood plasma in diagnostics and differentiation of pathological states of human organism of various nosology. *Appl. Opt.* 2014. **53**. P. B172–B180.
16. Ushenko A.G., Burkovets D.N., Ushenko Yu.A. Polarization phase mapping and reconstruction of biological tissue architectonics during diagnosis of pathological lesions. *Optics and Spectroscopy*. 2002. **93**, No. 3. P. 449–456.
17. Ushenko Yu.A., Tomka Yu.Ya. and Dubolazov A.V. Complex degree of mutual anisotropy of extracellular matrix of biological tissues. *Optics and Spectroscopy*. 2011. **110**. P. 814–819.
18. Gerrard A., Burch J.M. *Introduction to Matrix Methods in Optics*. New York, A Wiley-Intersci. Publ., 1975.
19. Angel'skii O.V., Ushenko A.G., Ermolenko S.B., Ushenko Yu.A., Pishak O.V. Polarization based visualization of multifractal structures for the diagnostics of pathological changes in biological tissues. *Optics and Spectroscopy*, 2000. **89**, No. 5. P. 799–804.
20. Goodman J.W. Statistical properties of laser speckle patters. In: *Laser Speckle and Related Phenomena*, Ed. J.C. Dainty. Berlin, Springer-Verlag, 1975. P. 9–75.
21. Kakturskii L.V. Clinical morphology of acute coronary syndrome. *Arkh. Patol.* 2007. **69**. P. 16–19.

22. Ushenko V.A., Sidor M.I., Marchuk Y.F., Pashkovskaya N.V., Andreichuk D.R. Azimuth-invariant Mueller-matrix differentiation of the optical anisotropy of biological tissues. *Optics and Spectroscopy*. 2014. **117**, No. 1. P. 152–157.
23. Ushenko V.A., Zabolotna N.I., Pavlov S.V., Burcovets D.M., Novakovska O.Yu. Mueller-matrices polarization selection of two-dimensional linear and circular birefringence images. *Proc. SPIE*. 2013. **9066**, Eleventh International Conference on Correlation Optics. P. 90661X.
24. Ushenko V.A., Gorsky M.P. Complex degree of mutual anisotropy of linear birefringence and optical activity of biological tissues in diagnostics of prostate cancer. *Optics and Spectroscopy*. 2013. **115**, No. 2. P. 290–297.
25. Basso C., Calabrese F., Corrado D., Thiene G. Postmortem diagnosis in sudden cardiac death victims: macroscopic, microscopic and molecular findings. *Cardiovascular Res*. 2001. **50**. P. 290–300.
26. Pérez-Cárceles M.D., Noguera J., Jiménez J.L., Martínez P., Luna A., Osuna E. Diagnostic efficacy of biochemical markers in diagnosis post-mortem of ischemic heart disease. *Forensic Sci. Intern.* 2004. **142**. P. 1–7.
27. Ushenko Yu.A., Gorsky M.P., Dubolazov A.V., Motrich A.V., Ushenko V.A., Sidor M.I. Spatial-frequency Fourier polarimetry of the complex degree of mutual anisotropy of linear and circular birefringence in the diagnostics of oncological changes in morphological structure of biological tissues. *Quantum Electronics*. 2012. **42**, No. 8. P. 727.
28. Ushenko V.A. Complex degree of mutual coherence of biological liquids, in: *ROMOPTO International Conference on Micro- to Nano-Photonics III* (pp. 88820V-88820V), International Society for Optics and Photonics, 2013.
29. Martínez Díaz F., Rodríguez-Morlensín M., Pérez-Cárceles M.D., Noguera J., Luna A. and Osuna E. Biochemical analysis and immunohistochemical determination of cardiac troponin for the postmortem diagnosis of myocardial damage. *Histol. Histopathol*. 2005. **20**. P. 475–481.
30. Angelsky O.V., Polyanskii P.V., Hanson S.G. Singular optical coloring of regularly scattered white light. *Opt. Exp*. 2006. **14**, No. 17. P. 7579–7586.
31. Ushenko Yu.O., Dubolazov O.V., Karachevtsev A.O., Gorsky M.P., Marchuk Y.F. Wavelet analysis of Fourier polarized images of the human bile. *Appl. Opt.* 2012. **51**, No. 10. P. C133–C139.
32. Ushenko Yu.A., Ushenko V.A., Dubolazov A.V., Balanetskaya V.O., Zabolotna N.I. Mueller-matrix diagnostics of optical properties of polycrystalline networks of human blood plasma. *Optics and Spectroscopy*, 2012. **112**, No. 6. P. 884–892.
33. Ushenko Yu.A., Tomka Yu.Ya., Dubolazov A.V. Laser diagnostics of anisotropy in birefringent networks of biological tissues in different physiological conditions. *Quantum Electronics*. 2011. **41**, No. 2. P. 170–175.
34. Ushenko V.A., Koval G.D., Gavrylyak M.S. Mueller-matrices polarization selection of two-dimensional linear and circular birefringence images. *Proc. SPIE*. 2013. **8856**, Applications of Digital Image Processing XXXVI. P. 88562E.
35. Gavrylyak M.S., Grygoryshyn P.M. The correlation-optical method measuring time of thrombus formation. *Proc. SPIE*. 2013. **9066**, Eleventh International Conference on Correlation Optics. P. 90661U.
36. Gavrylyak M.S. Correlation method for measuring the largest Lyapunov exponent in optical fields. *Ukr. J. Phys. Opt*. 2008. **9**, No. 2. P. 119–127.
37. Angelsky O.V., Ushenko A.G., Ushenko Y.G. Complex degree of mutual polarization of biological tissue coherent images for the diagnostics of their physiological state. *J. Biomed. Opt.* 2005. **10**, No. 6. P. 060502–060502-3.
38. C.S. Davis, *Statistical Methods of the Analysis of Repeated Measurements*. New York, Springer-Verlag, 2002.
39. A. Petrie, B. Sabin, *Medical Statistics at a Glance*. Blackwell Publishing, 2005.